Journal of Sound and Vibration (1999) **225**(1), 171–187
Article No. jsvi.1999.2229, available online at http://www.idealibrary.com on IDEAL®

NEW ACOUSTIC AND AERODYNAMIC PHENOMENA DUE TO NON-UNIFORM ROTATION OF PROPELLERS

J. P. Yin, S. R. Ahmed and W. Dobrzynski

DLR, Institute of Design Aerodynamics, Technical Acoustics, Lilienthalplatz 7, 38108 *Braunschweig, Germany*

(*Received* 16 *April* 1998, *and in final form* 26 *February* 1999)

A study is reported of the influence of non-uniform rotation—which is inherent to piston engine driven propellers—on the aerodynamics and aeroacoustics of multi-blade propellers by numerical simulation. The combination of aerodynamic predictions with a 3-D unsteady free wake panel method and aeroacoustic predictions based on Farassat's Formulation 1A of the Ffowcs Williams and Hawkings equation is used to achieve this goal. The numerical results show that non-uniform rotation has a significant influence on propeller aerodynamics and can lead to an increase in the generated noise. In case of a mismatch between the periodicity of the non-uniformity and the basic blade passage frequency, additional harmonics ("subharmonics") are generated. For a periodicity coincidence, the effects are masked due to an overlapping of the frequencies. The level of such subharmonics may be high enough to increase the overall A-weighted noise. The azimuthal directivity of the of the propeller noise remains no longer axisymmetric, and changes to a wave-like harmonic variation. The number of undulations per revolution depends on the order of the non-uniformity and is not related to the number of propeller blades. The polar directivity pattern also changes substantially from that known for uniform rotation. A frequency domain analysis of the unsteady pressure distribution shows that the subharmonics perceived at a space-fixed location are not due to an aerodynamic or acoustic interaction but rather the consequence of a motion geometry or Doppler effect.

1. BACKGROUND

Rising concern for aviation noise as a source of community annoyance has led to the introduction of increasingly stringent noise certification for all aircraft. To meet the permitted noise levels for piston engine-driven propeller aircraft, both the engine and the propeller are under scrutiny with the aim to develop new designs which reduce the noise emission levels with a minimum of penalty in performance.

To exploit fully the noise reduction potential, all components of the propeller drivetrain—engine with its accessories, muffler, engine mounting, etc.—as well as the structural environment and flow conditions in which the propeller operates, have to be considered. The present work addresses a part aspect of this complex and multi-disciplinary problem, prompted by a recent finding by Dobrzynski and

0022-460X/99/310171 + 17 $30.00/0

Gehlhar [1, 2]. They found that the non-uniform propeller rotation produced by the piston engine drive causes a periodic variation of blade loading. This generates noise in excess to that observed during uniform (electrical motor driven) propeller rotation. Further, they found that for some special combinations of number of blades and order of non-uniformity, some "non-propeller-harmonic" tones can be observed, which were explained to be generated by aeroacoustic interaction.

A somewhat similar phenomena was reported by Kameier and Neise [3] who, while investigating the noise source mechanisms in blade tip clearance region of axial flow turbines, noticed a flow instability which rotates slower than the impeller. This flow instability was identified as a contributor of extra tone components in the noise spectrum.

The objective of the work presented here is to analyze the effect of the order and amplitude of a rotation non-uniformity on the characteristics of the noise generated by a propeller. The basis of this study is a theoretical approach whereby the unsteady aerodynamics of a non-uniform rotating propeller are calculated and fed into an aeroacoustic code to obtain the noise radiation characteristics. A single harmonic non-uniformity of a particular order and amplitude is used at a time to perturb the uniform rotation aerodynamics of the propeller. This is done on a set of three propellers with two, three and five blades with diameters of 1·9, 1·8 and 1·6 m, respectively. Each of these propellers was designed to produce a thrust of 2300 N at 2700 r.p.m. by a procedure developed by Hepperle [4]. Only the propellers with two and five blades were available as hardware and were used during wind tunnel and flight tests. The three blade propeller was a theoretical design and used as such for the parametric investigations.

Variation of the order of perturbation harmonic or alternatively the number of blades allows a study to be made of the effect of the presence or absence of a coincidence between periodicity of the perturbation and the blade passage frequency. A further objective pursued was to clarify the physical mechanism behind the generation of additional (sub-)harmonics by using a simple frequency domain analysis.

2. DESCRIPTION OF THE METHOD

2.1. THE AERODYNAMICS CODE

Panel methods are numerical schemes for the solution of potential flow problems and are capable of treating subsonic (incompressible) flows about complex three-dimensional configurations. The concepts to simulate flow around propellers with this method are well known and documented in the literature (see e.g. references [4, 5]). In the specific case of unsteady flow, the boundary condition of flow tangency on the blade surface at every instant in time needs to be satisfied by the solution. A detailed description of the 3-D unsteady free wake panel method used for the computations in this paper is given in reference [6].

The model of the lifting propeller blade used here (at any time instant) consists of (see Figure 1) the following: (1) a source/sink distribution over the blade surface to simulate the displacement effect of the blade of *finite thickness*; (2) a *prescribed*

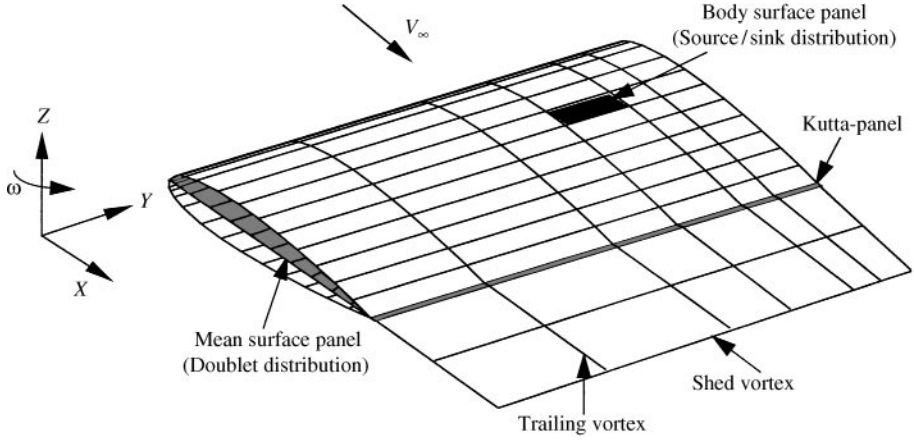

Figure 1. Numerical model of the blade and wake segment.

variation of the vortex strength over the blade section mean line to simulate the lift generation by the blade; (3) a short zero-thickness elongation of the blade trailing edge (*Kutta panel*) along its bisector to fix the direction of the shed (wake) vortex and the strength of blade circulation.

The numerical procedure consists of dividing the blade,- and the mean surface into small planar surface elements (panels), which carry a source/sink or vorticity distribution, respectively, of unknown strength. Imposing the flow tangency condition at a collocation point on the blade surface and the Kutta panels leads to a system of *linear* algebraic equations whose iterative solution gives the source/sink or vorticity strengths at the panel collocation points for each time (computation) step.

Summing up the induced velocity contributions from all source/sink and vortex strengths at a collocation point (e.g. of a panel on the blade surface) gives the total induced velocity prevalent there. To this is added the velocity due to rotation and translation of the collocation point to arrive at the value of the total velocity. With the velocity at collocation points of all panels comprising a chordwise blade strip evaluated this way, the corresponding pressure distribution around the blade profile is calculated by using the *unsteady* Bernouli equation. The integration of this pressure distribution gives the section lift for the blade at that radial station.

After each time step, vortex elements are shed from the Kutta panel trailing edge and are moved downstream with the current value of the total velocity (pertaining to the particular vortex element) over the duration of the next time step. A contiguos "free wake" is generated in this manner behind the blade trailing edge.

It should be noted here that the "unsteady" aerodynamic solution is in reality a sequential grouping together of a set of "quasi-steady" solutions, each satisfying the instantaneous boundary conditions of the time-dependent flow.

2.2. THE AEROACOUSTICS CODE

Propeller noise predictions were attempted as early as 1919 when Lynam and Webb [7] developed a numerical model for the propeller consisting of rings of sources and sinks. Although Gutin [8] and Deming [9] realized that propeller noise has both thickness and loading noise components, the real progress in noise prediction came after Lighthill [10] developed the acoustic analogy concept.

Today, most of the noise-prediction methods are based on the Ffowcs Williams and Hawkings (FWH) equations [11], which is the integral form of the acoustic analogy. Farassat's formulations [12] for noise prediction that are widely used by both propeller and helicopter industry are the FWH equation in formats suitable for implementation in modern computer algorithms. Metzger [13] provided recently an in-depth history and review of propeller noise prediction methodology.

The aeroacoustics code developed by the authors [14] and used to analyze the propeller acoustics in the present work is also based on the formulation 1A of Farassat [12], with consideration of thickness and loading terms only. Quadrupole noise is believed to be small compared to thickness and loading noise in the incompressible propeller flow under study. The code, which was originally written to predict the discreet frequency noise of helicopter rotors and propellers, was extended to simulate a time-dependent rotation of the propeller. The computations are performed in the time domain resulting in an acoustic pressure time history which is then Fourier-analyzed to obtain the sound pressure level and the acoustic spectrum.

In the case of potential flow, the formulation 1A of Farassat can be written as

$$4\pi P'_T(\vec{x}, t) = \int_{f=0} \left[\rho_0 C_0^2 \frac{\dot{M}_n}{C_0 r (1 - M_r)^2} \right]_{\text{ret}} \mathrm{d}S + \int_{f=0} \left[\rho_0 C_0^2 \frac{M_n (r \dot{M}_i \hat{r}_i + C_0 M_r - C_0 M^2)}{C_0 r^2 (1 - M_r)^3} \right]_{\text{ret}} dS, \tag{1}$$

$$4\pi P'_L(\vec{x}, t) = \int_{f=0} \left[\dot{P} \frac{\hat{n}_i \hat{r}_i}{C_0 r (1 - M_r)^2} \right]_{\text{ret}} \mathrm{d}S + \int_{f=0} P \left[\frac{\dot{\hat{n}}_i \hat{r}_i}{C_0 r (1 - M_r)^2} + \frac{\hat{n}_i \hat{r}_i - \hat{n}_i M_i}{r^2 (1 - M_r)^2} + \frac{\dot{\hat{n}}_i \hat{r}_i (r \dot{M}_i \hat{r}_i + C_0 M_r - C_0 M^2)}{C_0 r^2 (1 - M_r)^3} \right]_{\text{ret}} \mathrm{d}S. \tag{2}$$

Here P'_T and P'_L denote the acoustic pressure due to thickness and loading noise respectively. The sum of both terms is the total acoustic pressure at the location $\vec{x}$ at time t. The integration is carried out over the area element $\mathrm{d}S$ on the surface $f = 0$, which represents the blade surface. The subscript 'ret' denotes that the integrals are to be evaluated at a retarded time and ρ_0 and C_0 are the density and speed of sound of the undistributed medium respectively. M is the local Mach number and the r the distance between a point on the blade surface and the observer location. The subscripts n and r represent quantities normal to the blade surface and in the

direction of radiation, respectively. A "$\hat{}$"-sign on n and r indicates the unit vectors in these directions. The dots on some variables represent their (source-) time derivatives. P is the unsteady surface pressure on the blade obtained from the aerodynamics code.

The calculation of the noise is performed as follows. First, the propeller blade surface is divided into a number of flat panels. This discretization of the blade surface is *denser* than that used for the aerodynamic calculations, (see below). Next, the retarded time is calculated for a specified observer time at all blade panel collocation points by an iterative solution of the retarded time equation $\tau = t - r/C_0$ where τ is the source time, t the observer time, r is the distance between the source and the observer, and C_0 the speed of sound. If the variation in rotational speed is known (for example from a blade-mounted accelerometer, as explained in section 3.2 below), this can be used to adjust the calculated retarded time. In this way, also the time derivative of the Mach number [$\dot{M}$ in equations (1) and (2)] can be determined. Both thickness and loading noise contributions can be influenced by this Mach number variation, as shown by Lowson [15]. The output of the aerodynamics code, as may be recalled, provides the unsteady pressure from which its time derivative [$\dot{P}$ in equations (1) and (2)] can be evaluated numerically.

The azimuth angle related to the retarded time is computed subsequently and then the corresponding blade surface pressure for this retarded-time blade position is determined. A *higher* panel density and *smaller* time steps are used to generate the unsteady pressure data set employed for the aeracoustic calculations. This implies the generation of additional *intermediate* pressure values by using spline interpolation techniques from the aerodynamics code output, which is obtained with a *less* dense panelling and *larger* time steps. This approach is adopted to enhance the fidelity of the aeroacoustic prediction. The propeller radiated noise is calculated by using equations (1) and (2). Finally, the sound pressure at an observer position $\vec{x}$ and observer time t is given by the sum of the contributions from all panels on the propeller blade surface.

A more detailed description of the aeroacoustics code is available in reference [14].

3. RESULTS AND DISCUSSION

3.1. PROPELLER AERODYNAMICS

The panel code was first used to predict the pressure distribution over a *uniformly* rotating propeller as a validation excercise and demonstration of the code capability. Figure 2 shows a comparison of the predicted pressure distribution for a two blade NACA 10-(3)(066)-033 propeller with experimental data of Maynard and Murphy [16]. Shown is the variation of the pressure coefficient C_p over the blade chord x/c at a number of radial stations r/R. Two sets of experimental data, corresponding to advance of 1·986 (symbol = circle), or 2·098 (symbol = square) are plotted, which approximately match the advance ratio value (= 2·0) of the computations. As seen, the predicted pressure distribution agrees quite well with the mean pressure data from the two advance ratios.

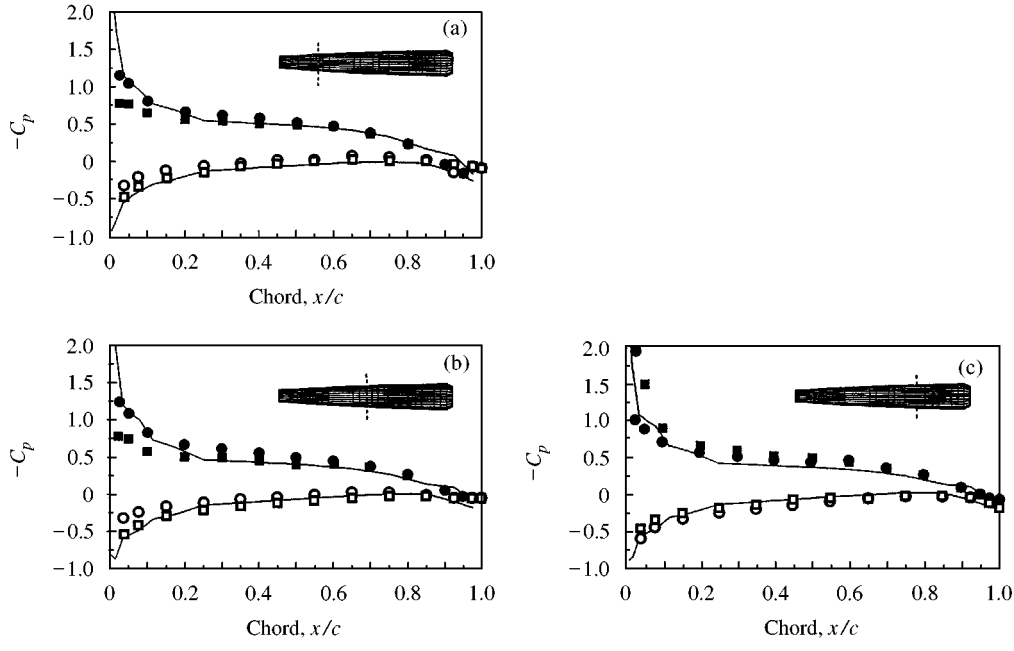

Figure 2. Pressure distribution over blade chord at various radial stations. Uniformly rotating two blade NACA 10-(3)(066)-033 propeller. Advance ratio = 2. —, Present code; ● ○ ■ □, experiment [16]. r/R values: (a) 0·45; (b) 0·65; (c) 0·78.

As mentioned earlier, the panel method used employs a free (= no load carrying) wake over the entire blade span. An impression of the wake pattern generated during the simulation is presented in Figure 3, where an instantaneous plot of the wake after two revolutions for a three-blade propeller in isometric view is shown. The azimuthal step size of the computations is 5°, which corresponds to a time step of 0·00031s for the propeller rotating with a r.p.m. of 2700. At the start of the computation, the wake is not present. With each computation step a wake segment is released at the trailing edge of the blade and aligns itself with the global flowfield. The downstream edge of the wake segment is moved downstream with a total velocity with contributions of induced velocity from the blade surface- and wake panel singularities as well as the velocity due to rotational and translatory motion of the propeller blade. This movement is done over the time interval of the computation step whereby the wake segments from earlier computation steps are moved contiguously downstream. The wake becomes progressively longer as the computation proceeds, with the addition of new segments. After each time step, the total wake is realigned with the current global flow field, and thus constitutes a no-load carrying "free wake".

3.2. AEROACOUSTIC RESULTS

As a next step the aerodynamics and aeroacoustics of a two-blade round tip general aviation aircraft propeller, which has been extensively tested in the

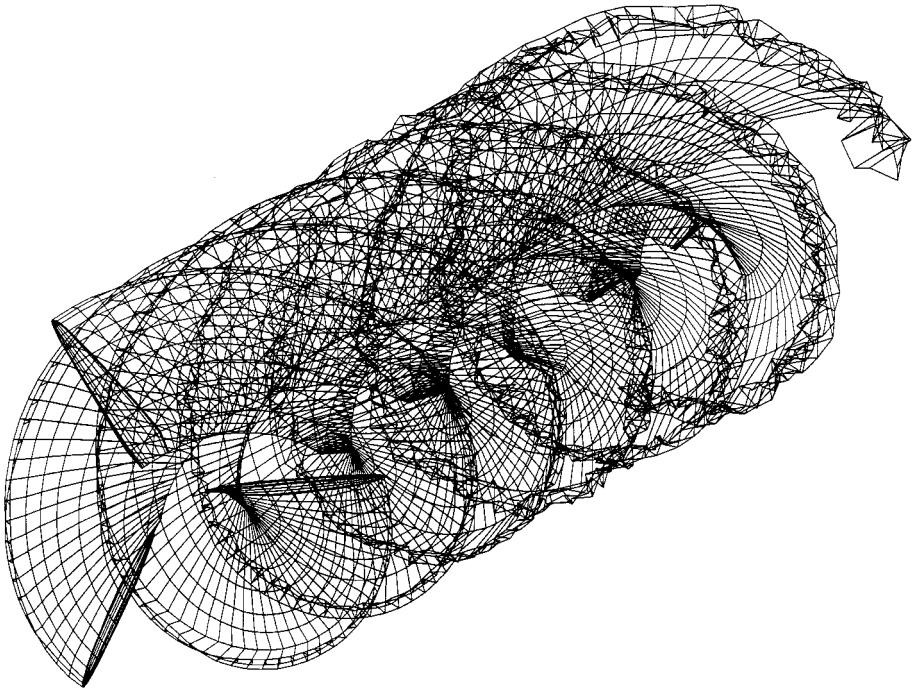

Figure 3. Free wake generated during the computation for the three-blade propeller.

German–Dutch Wind Tunnel (DNW) by Dobrzynski *et al.* [17], were calculated. The propeller was rotated uniformly with an electric motor during the tests. Figure 4 shows a comparison of predicted and measured sound pressure (*SP*) time history and the corresponding results for the discreet sound pressure level (*SPL*) spectra at the in-rotation-plane location (microphone 4), and the $\phi = -40^\circ$ polar angle location (microphone 7). The *SP* time history data from experiment exhibits some contamination due to reflections from the microphone support structure, as noted in reference [17]. Otherwise, the correlation between the computed and measured *SP* time history for this uniform rotation case is good. Also, the *SPL*s are in good agreement with the experimental data which is denoted by open circles. However, the *measured* spectrum (symbol = open circles) contains subharmonics which could be the contribution of *extraneous* noise sources and reflections present in the wind tunnel and test section area.

A more critical test of the code was the simulation of the aerodynamics and aeroacoustics of a five-blade propeller is non-uniform rotation, which was subjected to flight and wind tunnel tests. During the flight tests, this propeller was fitted to and driven by a 4-stroke 4-cylinder piston engine of a small general aviation aircraft and its flyover noise characteristics were measured. One blade of the propeller was instrumented with an accelerometer so that quantivative acceleration measurements were possible during the flight tests. The averaged value of the acceleration data acquired over a large number of revolutions defined the non-uniform acceleration experienced by the blade. From a time integration of this

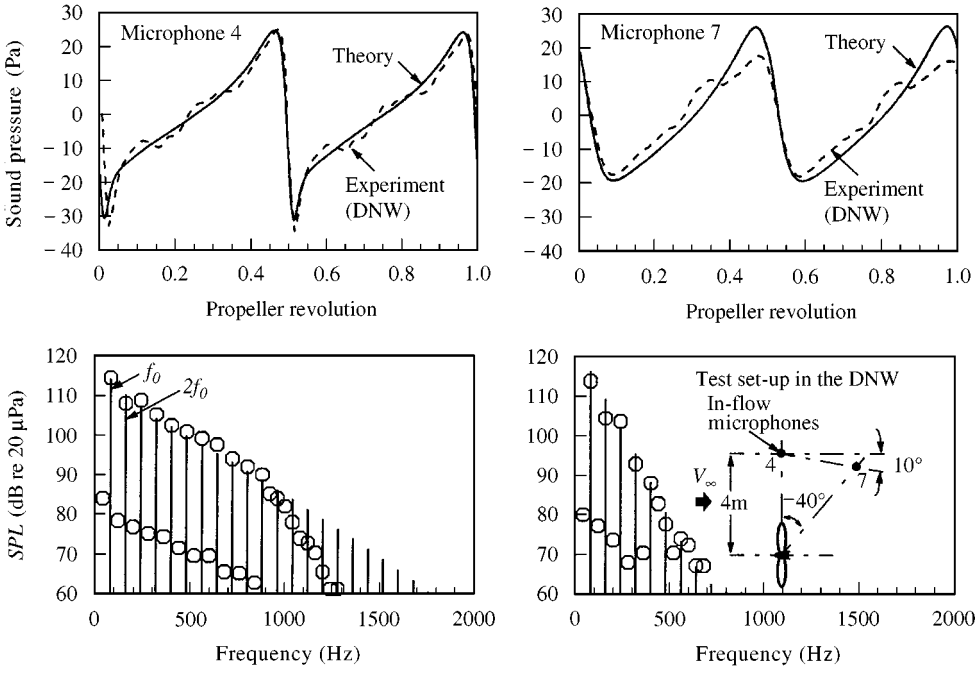

Figure 4. Sound pressure time history (top) and sound pressure level spectrum (bottom) at two microphone locations. Comparison of predictions with DNW measurements [17]. Two-blade propeller in uniform rotation, $BPF = 90$ Hz, $V_\infty = 51{\cdot}5$ m/s. —, Theory; ○, experiment (DNW).

acceleration data, performed numerically, the magnitude of the non-uniform rotation speed was determined.

Next, the propeller was fitted on to a test rig in the DNW and driven by the same aircraft engine and its aeroacoustics were measured in the wind tunnel. Both the flight- and the wind tunnel tests revealed the existence of high *SPL* at the 6th (f_6), 11th (f_{11}) and 16th (f_{16}) harmonics of the shaft rotational frequency f_0, which was, as noted earlier, a totally unexpected result obtained from the experiments.

The measured rotation non-uniformity from the flight tests was Fourier-analyzed and its first 18 harmonics were used to introduce a non-uniformity in the aerodynamic computations for the five-blade propeller. This reproduced the measured non-uniformity of the flight tests with sufficient accuracy in the theoretical simulation.

To gain an insight into the mechanism of generation of the subharmonics, the predicted section lift coefficient of the five-blade propeller at three radial stations r/R is plotted over the number of revolutions in Figure 5 together with the result for uniform rotation. As evident, the non-uniformity generates an unsteady blade loading during the propeller rotation. The average value of this unsteady loading is higher than the corresponding value for uniform rotation especially for sections close to the blade tip.

Since the noise from the blade loading is essentially determined by its time derivative [as seen in equation (2)], in Figure 6 the behaviour of the spectra of the

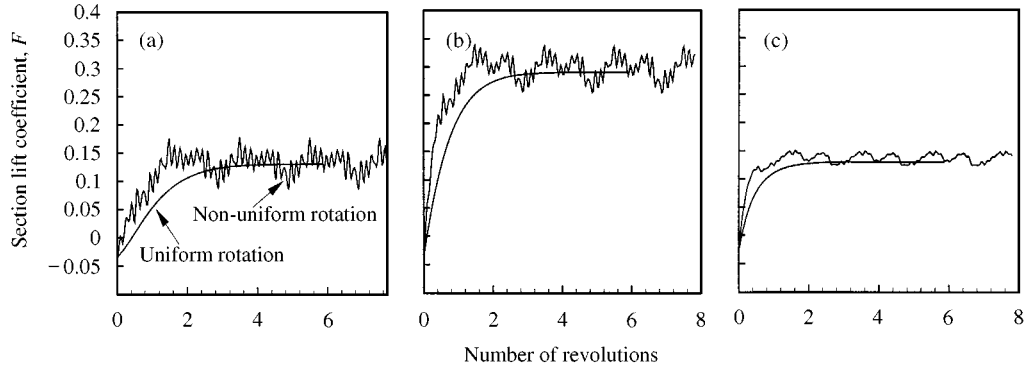

Figure 5. Time history of section lift coefficient at various radial stations. Predicted results for a five-blade propeller in uniform and non-uniform rotation. r/R values: (a) 0·23; (b) 0·50; (c) 0·96.

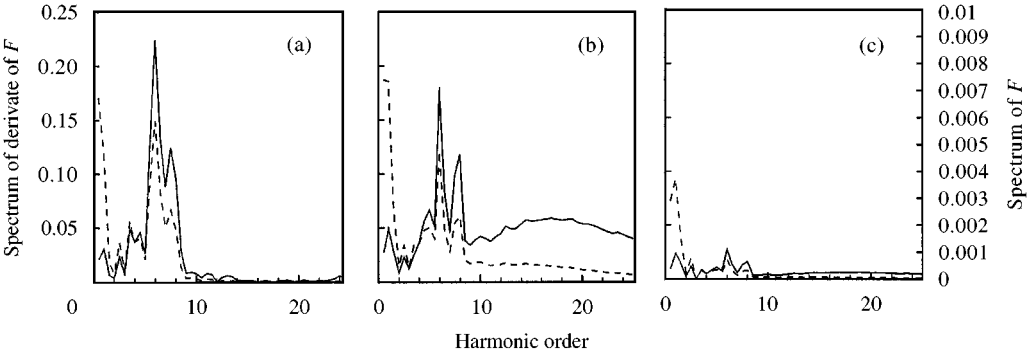

Figure 6. Spectrum of section lift coefficient and its derivative at various radial stations. Five blade propeller in non-uniform rotation. r/R values: (a) 0·23; (b) 0·50; 0·96. —, F'; – – – –, F.

section lift coefficient (F), and its time derivative (F') is examined. The spectrum for F (dashed-line), exhibits maxima at $f_{0\cdot5}$ and at f_6 at the stations $r/R = 0{\cdot}23$ and 0·5; at the station near the tip, $r/R = 0{\cdot}96$, a peak at f_1 is present. The spectrum for F' (full line), shows a different behaviour. The F' values for f_6 are the highest at the first two r/R-stations; at $r/R = 0{\cdot}96$, both f_1 and f_6 have nearly the same value. The generation of extra harmonics at f_1 and f_6 is believed to be caused by this behaviour of the F'-spectrum. Dominance of f_6 seems to be a characteristic property of this particular 4-stroke engine.

Figure 7 shows the computed SP history and SPL spectrum for the five-blade propeller. Also shown are results from DNW measurements for an observer position 'P' as indicated on the top right in the figure. The imposition of a "real-life" non-uniformity on the uniform rotation radically distorts the SP time history. The time history pattern repeats itself after two revolutions, which is typical for a 4-stoke engine. A look at the corresponding computed SPLs (Figure 7, middle) shows the generation of numerous subharmonics which have their counterparts also in the measured spectrum, as seen in the lower diagram of Figure 7. The excessive SPLs noticed in the experiment for the frequencies f_6, f_{11}, f_{16}, etc.,

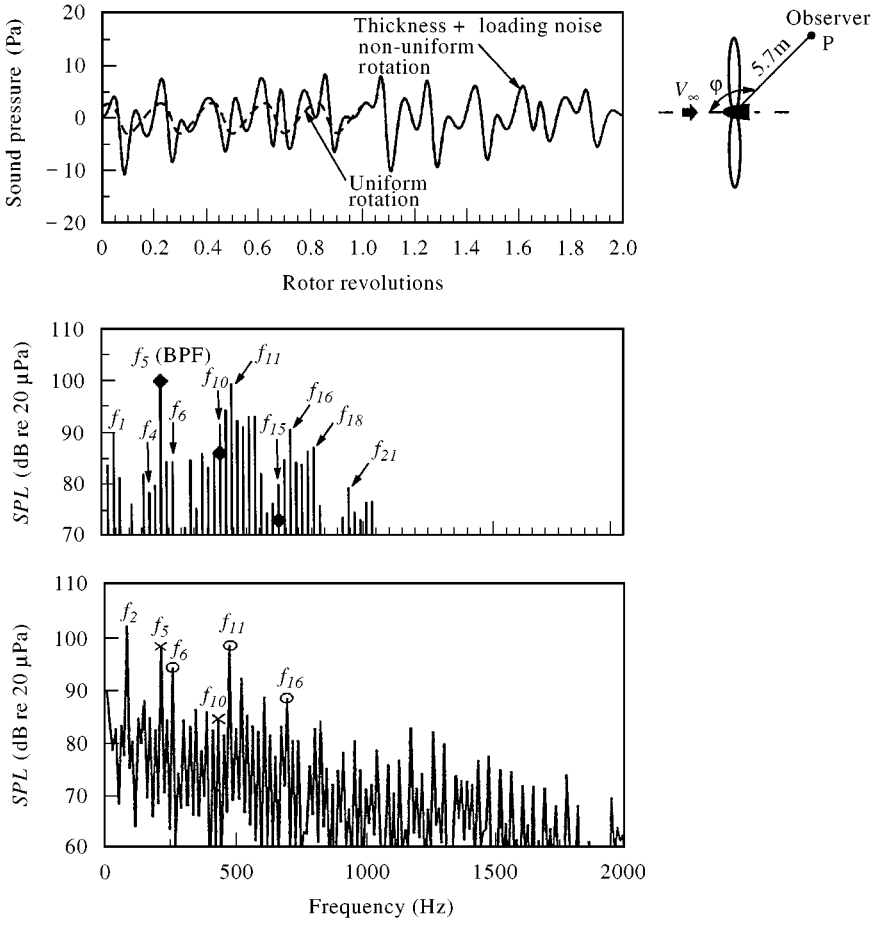

Figure 7. Sound pressure history (top), predicted sound pressure level spectrum (middle), and sound pressure level spectrum (bottom) measured in DNW tests [2]. Five blade propeller rotating with "flight data" non-uniformity; $BPF = 225$ Hz, $V_\infty = 77$ m/s. For middle: ◆, uniform rotation; —, non-uniform rotation. For bottom: ×, uniform rotation harmonics; ○, sub-harmonics.

especially at f_{11} and f_{16}, have been successfully duplicated by the numerical simulation. The subharmonics at f_1 and f_6 are believed to be generated by the corresponding pressure derivate peaks of Figure 6, as discussed earlier. An explanation for the occurrence of the subharmonics with high SPL such as f_{11} and f_{16} is attempted in the next section (section 4.1). This example demonstrates that non-uniform rotation can directly contribute to the noise through subharmonics which are generated in addition to the harmonics of uniform rotation.

4. THE GENERATION OF SUBHARMONICS

4.1. PERTURBATION ANALYSIS

The characteristics of the pressure distribution on the blade have a strong bearing on the noise emission from the propeller. In the case of non-uniform

rotation, the pressure P is time dependent in the blade fixed frame of reference. Under the assumption of small perturbations it can be expressed as

$$P(\theta', t) = P_0(\theta') + \sum_{n=1}^{\infty} \Delta P(\theta') \cos(n\omega_0 t + \phi_n), \tag{3}$$

where n is the order of the perturbation harmonic referred to the shaft rotational frequency $\omega_0 = 2\pi f_0$ and $\Delta P(\theta')$ and ϕ_n are the perturbation harmonic amplitude and its phase respectively. $P_0(\theta')$ represents the steady loading on the blade which can be obtained from the time average of equation (3). To obtain the pressure fluctuation at a location fixed in space and lying in the plane of rotation, equation (3) can be transformed to a space-fixed frame of reference, by using the transformation $\theta = \theta' + \omega_0 t$, where θ and θ' are azimuth angles defined in the space- and blade-fixed frame of reference, respectively. For the sake of simplicity, only a single-harmonic perturbation of the order $n\omega_0$ is considered, so that the effect of non-uniform rotation on ω_0 in the transformation is neglected. If there are B blades on the propeller, spaced $2\pi/B$ radians apart, the associated pressure variations are repeated after this interval. Equation (3) can be represented by a Fourier series as

$$P(\theta, t) = \sum_{m=0}^{\infty} A_m \cos[mB(\theta - \omega_0 t) + \phi_m] + \sum_{m=1}^{\infty} B_m \cos[mB(\theta - \omega_0 t) + \phi'_m] \cos(n\omega_0 t + \phi_n), \tag{4}$$

where A_m, B_m and ϕ_m, ϕ'_m are the amplitude and phase parameters of the Fourier transformation, respectively, and m the order of the perturbation in the space-fixed frame of reference. In equation (4), the first and second terms result from the Fourier transformation of the first and second terms in equation (3). By a simple rearrangement (upon neglecting for the sake of simplicity the phase parameters) one obtains from equation (4).

$$P(\theta, t) = \sum_{m=0}^{\infty} A_m \cos[mB(\theta - \omega_0 t)] + B_m \{\cos[mB\theta - (\mathrm{m}B - n)\omega_0 t] + \cos[mB\theta - (mB + n)\omega_0 t]\}. \tag{5}$$

As explained in standard text books of acoustics (see e.g. reference [18]), a modal analysis of this equation says that besides the mB lobed spinning modes rotating at ω_0, there are additional mB lobed spinning modes rotating at angular velocities $(mB + n)\omega_0/(mB)$ and $(mB - n)\omega_0/(mB)$. Therefore, non-uniform rotation will generate extra spinning modes and create extra (pressure fluctuation) harmonics at the frequencies

$$(mB + n)\omega_0 \quad \text{and} \quad (mB - n)\omega_0. \tag{6}$$

The extra harmonics perceived at a space-fixed location are thus not a consequence of an aerodynamic or acoustic interaction phenomena but simply a

geometry or Doppler effect created by the transfer of the non-uniformity from a blade-fixed to a space-fixed observer position. The non-uniformity in the blade-fixed frame of reference is transformed into a different non-uniformity in the space-fixed frame of reference. The extra harmonic pressure disturbance generated in the space-fixed frame of reference, propagates then as additional noise.

In case of a mismatch between the periodicity of the non-uniformity and the basic blade passage frequency (*BPF*), for example, a five blade propeller ($B = 5$, $BPF = 5\omega_0/2\pi$), operating with a non-uniformity of sixth order ($n = 6$), will according to equation (6) and with $m = 1, 2, 3, \ldots$, generate subharmonics of the order of 6, 9, 11, 16, … , which will add to the radiated noise. When the order of non-uniformity is changed, then the order of subharmonics generated is also changed.

4.2. PARAMETRIC STUDY

To get a deeper insight into the effect of non-uniform rotation on the aeroacoustics of propellers, the characteristics of the non-uniformity were systematically changed. To this effect, a single-harmonic perturbation of a particular order and amplitude was imposed on the uniform rotation such as that

$$\omega(\chi)/\omega_0 = 1 + A_n \cos(n\omega_0 t). \tag{7}$$

Here ω denotes the instantaneous- and ω_0 the uniform rotational frequency, χ the azimuth angle, A_n the amplitude, n the order of the perturbation harmonic (referred to f_0), and t the time.

4.2.1. *Effect of the order of perturbation*

As representative result of the effect of the order of the perturbation harmonic 'n' on the propeller aeroacoustics, Figure 8 shows the *SP* time history for one revolution and the corresponding *SPL* spectrum for a three-blade propeller operating at 2700 r.p.m. The upper two plots depict results for $n = 2$ and the lower two for $n = 6$. In both cases the amplitude of the perturbation A_n was 1% of ω_0.

In case of a mismatch between blade passage frequency (*BPF*) and n (for example $BPF = 3f_0$, and $n = 2$ for the top right plot in Figure 8), subharmonics of the order $f_1, f_2, f_4, f_5, f_7, f_8$, etc., are generated. These are in addition to the harmonics for uniform rotation, viz., $f_3, f_6, f_9, \ldots$, etc. The *SPL*s for uniform rotation are indicated by "diamond" symbols in Figure 8. It is interesting to note that the subharmonics $f_5, f_8, f_{11}, \ldots$, exhibit significant *SPL*s, which decay slower than the "steady" harmonics $f_3, f_6, f_9, \ldots$.

The bottom right plot in Figure 8 shows the results for a coincidence between (twice) the *BPF*, which is 6, and n. This matching between the frequencies prevents the generation of subharmonics. The perturbation generates subharmonics which *overlap* with the *BPF* or its integer multiples, thus masking the magnitude of their contribution. A comparison with the *SPL*s for uniform rotation—indicated by "diamond" symbols—shows that a modulation of the *SPL*s does take place, and this may even lead to a decrease in *SPL*s at certain frequencies.

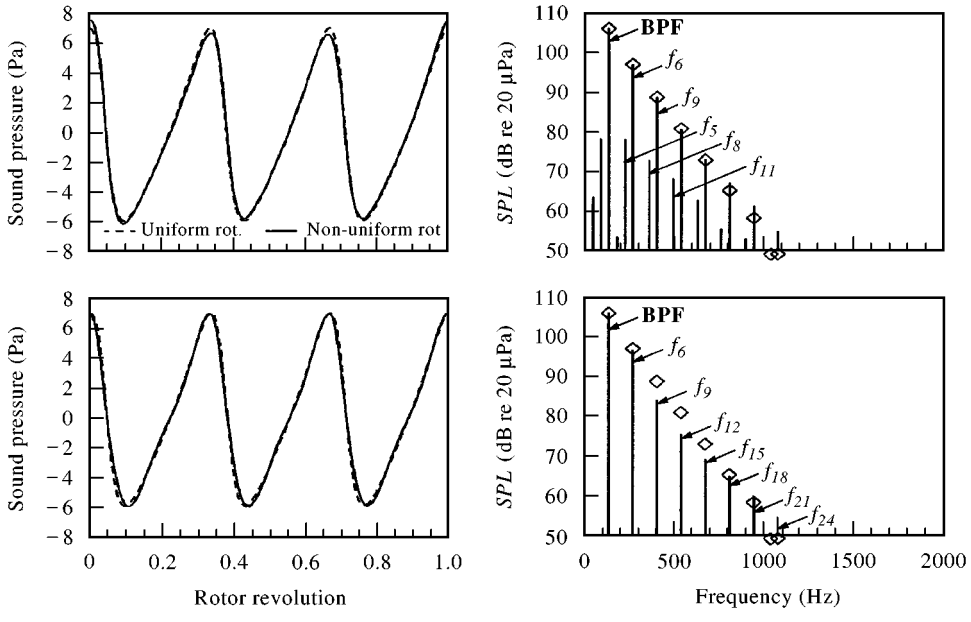

Figure 8. Effect of the order of perturbation harmonic on the sound pressure time history and sound pressure level spectrum. Top row: $n = 2$, $A_n = 1\%$, bottom row: $n = 6$, $A_n = 1\%$. Predicted results for three blade propeller in uniform (◇) and non-uniform (—) rotation. $BPF = 135$ Hz.

The results for the *SP* time history in Figure 8 are less dramatic; the variation for the uniform rotation (broken line) deviates only slightly near the maxima and minima from the curve for the perturbed rotation. However, the generation of the harmonics seen in the spectrum is the consequence of the change in the *gradient* of the *SP* time history, which is obviously more significant than can be discerned from the plots on the left in Figure 8.

4.2.2. *The effect of azimuthal observer location*

To bring out yet another effect of non-uniform rotation, Figure 9 shows the A-weighted *SPL* spectrum for a two-blade propeller at two azimuthal observer positions, namely at $\chi = 10^\circ$ and 35°. The uniform rotation is perturbed by a harmonic of $n = 6$ and amplitude $A_n = 2\%$. The *SPL*s for uniform rotation at 2700 rpm are indicated with "diamond" symbols. For the azimuthal observer location of $\chi = 10^\circ$ (and polar angle location $\varphi = 120^\circ$), the A-weighted *SPL*s in the range of 300–700 Hz are reduced and beyond 900 Hz increased over the values for uniform rotation. The situation at the same polar angle location but at an azimuth angle of $\chi = 35^\circ$ exhibits an increase in A-weighted *SPL*s for all frequencies above 300 Hz as compared to the values for uniform rotation.

Summarizing from Figures 8 and 9, one can say that a mismatch between *BPF* and *n* leads to generation of subharmonics which change the tonal quality of the noise. The effect of non-uniformity on the *SPL* can be high enough to alter the overall A-weighted noise level. Coincidence between *BPF* and integer multiples of *n* can result in an increase or decrease of A-weighted *SPL*s in the spectrum, depending on the azimuthal location of the observer.

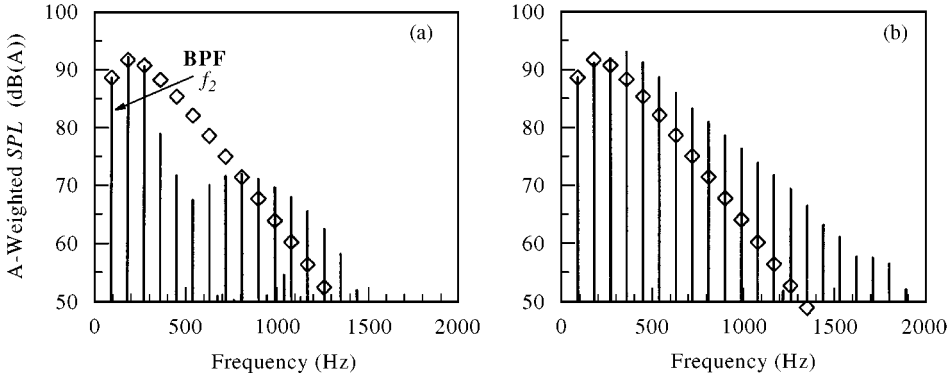

Figure 9. Variation of A-weighted sound pressure level spectrum with azimuth angle. Predicted results for two blade propeller in uniform (◇) and non-uniform (—) rotation. $BPF = 90$ Hz. $n = 6$, $A_n = 2\%$, $\varphi = 120°$. (a) $\chi = 10°$; (b) $\chi = 35°$.

4.2.3. *The effect of perturbation amplitude*

Figure 10 demonstrates the effect of a doubling of A_n on the *SP* time history and *SPL*s of the spectrum. Considered is a three-blade propeller rotating at 2700 r.p.m. with a perturbation of $n = 0{\cdot}5$ imposed alternatively with an amplitude $A_n = 1$ or 2%. The SPLs for $A_n = 1\%$ are indicated with an "asterisk" in the spectrum plot. Since *BPF* and *n* do not match in this case, subharmonics $f_{0{\cdot}5}, f_{2{\cdot}5}$ etc., are visible in the spectrum. The effect of a change in amplitude manifests itself, as expected, in a general increase in the *SPL*s of the individual subharmonics. *SPL*s for frequencies coinciding with *BPF* or its integer multiples, are reduced somewhat (for the non-uniform rotation) in the frequency range above 800 Hz. The *SP* histories for the two different amplitudes (left plot of Figure 10) differ only slightly from one another.

4.2.4. *Effect of non-uniform rotation on azimuthal directivity*

An interesting effect of the rotation non-uniformity is the change in the azimuthal directivity as evident in the plot of Figure 11 where the *SPL*s for the frequencies f_8, f_{10} and f_{12} are plotted over the azimuth angle χ. Considered is the two-blade propeller operating at 2700 r.p.m. with a perturbation of $n = 6$ and an amplitude $A_n = 2\%$. The observer location is at a polar angle of $\varphi = 120°$ on the rear side of the propeller plane of rotation.

While uniform rotation produces constant *SPL*s over the azimuth, the imposition of $n = 6$ non-uniformity generates a six per revolution periodic variation of *SPL* for all the frequencies considered. The relative increase in the *SP* (over the value for uniform rotation) turns out to be higher for the higher frequency (e.g. f_{12}) than for the lower frequencies. The omni-directional character of the azimuthal directivity is changed thus to a *n*-coincident periodic function.

4.2.5. *Effect of non-uniform rotation on polar directivity*

Figure 12 shows results of the polar directivity for three frequencies viz. f_8, f_{10} and f_{12} for the two-blade propeller operating under conditions described in

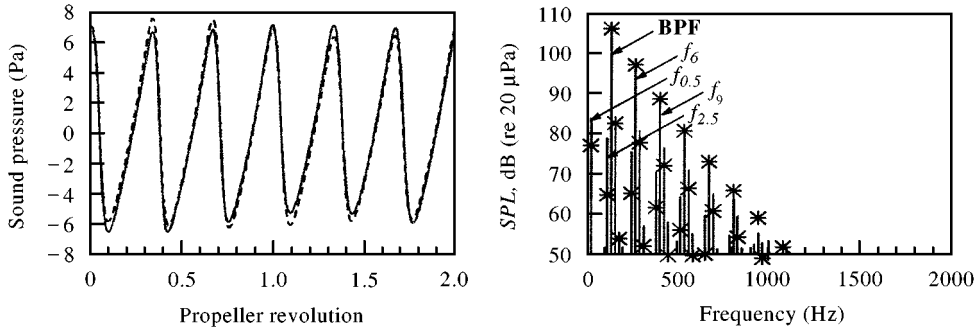

Figure 10. Effect of perturbation harmonic amplitude on sound pressure time history and sound pressure level spectrum. Predicted results at polar angle location of 120 degrees. Three blade propeller in non-uniform rotation. $BPF = 135$ Hz, $n = 0.5$. A_n values: – – –, ∗, 1%; —, 2%.

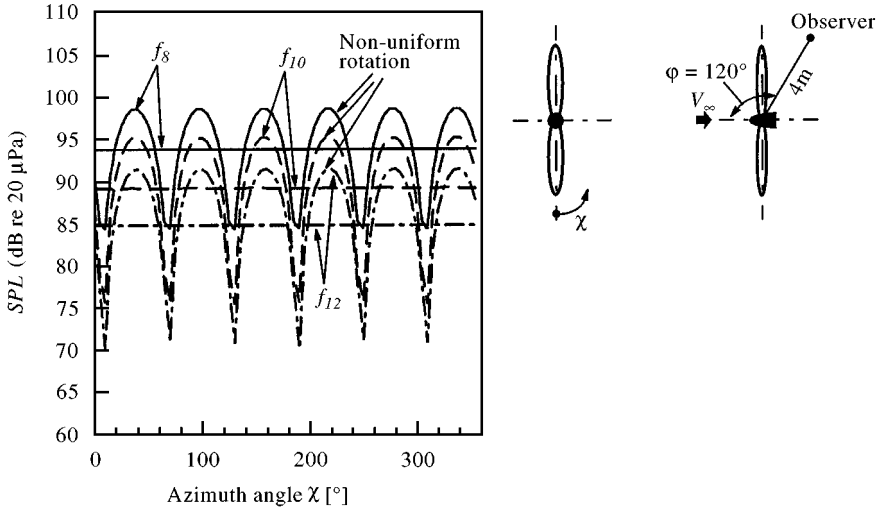

Figure 11. Effect of harmonic perturbation on azimuthal directivity, $n = 6$, $A_n = 2\%$. Predictions for two blade propeller in non-uniform rotation. —, – –, – – –, uniform rotation.

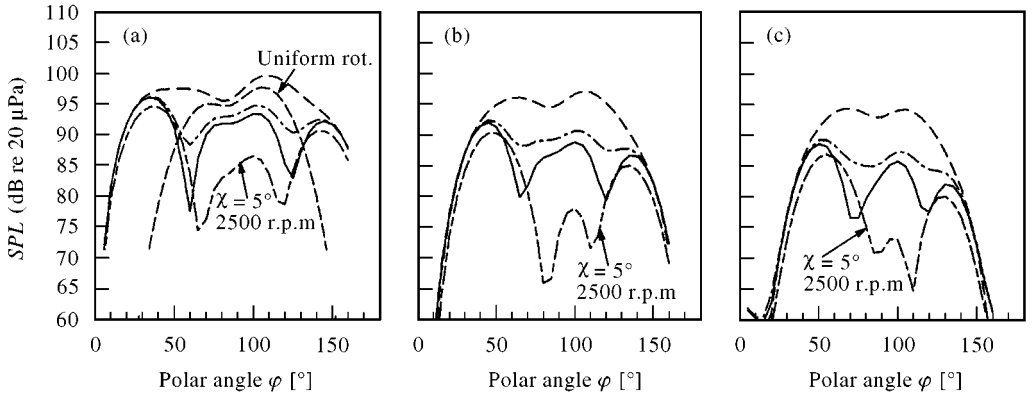

Figure 12. Effect of harmonic perturbation and rotational speed on polar directivity, $n = 6$, $A_n = 2\%$. Predictions for two blade propeller in uniform and non-uniform rotation. (a) f_8; (b) f_{10}; (c) f_{12}. For 2700 RPM: —, $\chi = 5°$, – – –, $\chi = 40°$; – –, $\chi = 60°$. Curves for 2500 RPM and $\chi = 5°$ as indicated on graphs.

previous section 4.2.4. Plotted in each frequency diagram are the directivity curves for the azimuth angles $\chi = 5$, 40 and 60°. Also shown (lowermost curve) is the directivity for $\chi = 5°$ at the reduced r.p.m. of 2500 but with the same value of n as for the higher r.p.m.

The non-uniformity distorts the polar directivity curve for uniform rotation—from a double peak curve, as shown for f_8 in the figure—to a curve with two to three peaks, with the peaks located ahead, at and in the rear of the propeller plane of rotation. The shape of the directivity curve depends on the azimuthal position and shows large *SPL* variation in the azimuth angle range of $\chi = 5$–60°. Significant variation of *SPL*s with polar angle is restricted to values of φ approximately between 40 and 140°. As seen in Figure 12, a reduction in the operating r.p.m. from 2700–2500 lowers the *SPL*s, particularly in the polar angle range between 60 and 120°.

5. CONCLUSIONS

Both for the uniform- and non-uniform rotation of propellers, the predicted results are in good agreement with the experimental data. The analysis shows that non-uniform rotation of the propeller significantly alters the propeller aerodynamics and can substantially increase the propeller noise and its tonal content.

In case of a mismatch between the periodicity of the non-uniformity and the blade passage frequency, subharmonics are generated which are in addition to the harmonics of uniform rotation. The contribution of these to the A-weighted noise level can be large enough to raise it above the value for the uniform rotation. Which of the subharmonics generated have an enhanced amplitude depends on the nature of the non-uniformity. Generally speaking, a non-uniformity has an adverse effect on the noise generation.

For a periodicity coincidence between the non-uniformity and the blade passage frequency (or its integer multiples), the effects on the noise spectrum are masked due to an overlapping of the frequencies. In this case also the amplitude of the individual frequencies may be raised or lowered which in turn alters the A-weighted sound level.

A simple perturbation analysis has shown that the generation of subharmonics is not due to an aerodynamic or aeroacoustic interaction phenomena but due to the non-uniformity-related change in blade kinematics with reference to a space-fixed observer.

The effect of an increase in the amplitude of the non-uniformity manifests itself in a general increase in the sound pressure level of the individual subharmonics.

Rotation non-uniformity changes both the azimuthal and polar directivity of the generated noise. While uniform rotation produces constant *SPL*s over the azimuth, the non-uniformity produces a "*n*-coincident" periodic variation of the *SPL* for all frequencies.

Polar directivity is changed by the non-uniform rotation in a way that higher *SPL*s are generated ahead and at the rear of the propeller plane. This change depends upon the azimuth angle considered. A reduction in the propeller r.p.m.

keeping the magnitude of non-uniformity constant, reduces the *SPL*s in the immediate neighbourhood of the propeller but not further ahead or in the rear.

REFERENCES

1. W. Dobrzynski and B. Gehlhar 1995 *INTER-NOISE* 95 *Proceedings*, *Newport Beach*, *USA*, 195–198. On the drastic propeller-noise increase due to (always present) engine crank-shaft rotational oscillation: A wind tunnel full-scale experimental demonstration.
2. W. Dobrzynski and B. Gehlhar 1997 3*rd AIAA-CEAS Aeroacoustics Conference*, *Paper No. AIAA-CEAS* 97-1708, *Atlanta/GA*, *USA*. The noise from piston engine driven propellers on general aviation airplanes.
3. F. Kameier and W. Neise 1997 *Journal of Sound and Vibration* **203**, 833–853. Rotating blade flow instability as a source of noise in axial turbomachines.
4. M. Hepperle 1992 *Ph.D. Thesis*, *Institut A für Mechanik*, *University of Stuttgart*, *Germany*. Ein Beitrag zur Aerodynamik des Propellers unter Berücksichtigung einer freien Nachlauffläche.
5. J. L. Hess, W. O. Valarezo 1985 *Journal of Propulsion* **I**, 470–476. Calculation of steady flow about propellers using a surface panel method.
6. S. R. Ahmed, V. T. Vidjaja 1994 50*th Annual Forum of the American Helicopter Society*. *Washington*, *DC*, *USA*, Unsteady panel method calculation of pressure distribution on BO 105 Model Rotor Blades and validation with DNW-test data.
7. F. J. Lynam and H. A. Webb 1918–1919 *Technical Report of the Advisory Committee for Aeronautics for the Year* 1918–1919, Vol. **11**. The emission of sounds by airsrews.
8. L. Gutin 1948 *NACA Technical Memorandum* 1195. On the sound field of a rotating propeller.
9. A. F. Deming 1940 *Journal of the Acoustic Society of America* **12**, 173–182. Propeller rotation noise due to torque and thrust.
10. M. J. Lighthill 1952 *Proceedings of the Royal Society*, *London* **211**, 564–587. On sound generated aerodynamically, I-general theory.
11. J. E. Ffowcs Williams and D. L. Hawkings 1969 *Philosophical Transactions of the Royal Society*, *London* **264**, 321–342. Sound generated by turbulence and surfaces in arbitrary motion.
12. F. Farassat 1975 *NASA TR*-451. Theory of noise generated from moving bodies and applications to helicopter rotors.
13. B. F. Metzger 1995 *NASA CR*-198156. A review of propeller noise prediction methodology.
14. J. P. Yin, S. R. Ahmed 1994 20*th European Rotorcraft Forum*, Paper No. 11, *Amsterdam*, *The Netherlands*. Prediction— and its validation—of the acoustics of multiblade rotors in forward flight utilising pressure data from a 3-D free wake unsteady panel method.
15. M. V. Lowson 1985 *Proceedings of the Royal Society*, *London* **A286**, 559–572. The sound field for singularities in motion.
16. D. Maynard, M. P. Murphy 1950 *NACA RM L9L*12. Pressure distributions on the blade sections of the NACA 10-(3)(066)-033 propeller under operating conditions.
17. W. Dobrzynski, H. Heller, J. Powers and J. Densmore 1986 *FAA Report No. AEE*-86-3, *Washington*, *USA*. DFVLR/FAA Propeller noise tests in the German–Dutch wind tunnel DNW.
18. M. E. Goldstein 1976 *Aeroacoustics*. New York: McGraw-Hill International Book Co.